

Molecular Dynamics Simulations of Field Emission From a Planar Nanodiode

Kristinn Torfason,¹ Agust Valfell,¹ and Andrei Manolescu¹

School of Science and Engineering, Reykjavik University, Menntavegur 1, IS-101 Reykjavik, Iceland

(Dated: 16 March 2015)

High resolution molecular dynamics simulations with full Coulomb interactions of electrons are used to investigate field emission in planar nanodiodes. The effects of space-charge and emitter radius are examined and compared to previous results concerning transition from Fowler-Nordheim to Child-Langmuir current^{1,2}. The Fowler-Nordheim law is used to determine the current density injected into the system and the Metropolis-Hastings algorithm to find a favourable point of emission on the emitter surface. A simple fluid like model is also developed and its results are in qualitative agreement with the simulations.

I. INTRODUCTION

Field emission of electrons from a metallic surface³⁻⁵ is an important process in vacuum electronics^{6,7}. Its primary use is for cold cathodes in applications such as microwave tubes, electron microscopes and flat panel displays. In addition to this beneficial application of field emission there are also negative implications, such as vacuum breakdown at high field strengths and dielectric surface breakdown initiated by field emitted electrons⁸.

The physical basis for field emission is that a strong applied electric field can deform the surface barrier of a metal-vacuum interface so as to increase the tunnelling probability to such a degree that a considerable current of electrons can be drawn from the surface. This process was first described by Fowler and Nordheim³ and has since been recast and extended for different applications. A particular area of interest is the effect of space-charge on field emission. Barbour et al. addressed this issue in 1953⁹, while Lau et al. conducted a study of transition from field emission to space-charge dominated emission in 1994¹. In both cases the approach was based on finding the equilibrium injection current that corresponds to the space-charge modified surface field. Feng and Verboncoeur² used a particle-in-cell code to simulate this problem, in which they used a detailed model that takes into account the effect of image-charge on the potential barrier for field emission. Rokhlenko et al.¹⁰ developed an elegant approach to calculate the effect of space-charge on field emission in a one dimensional system that included lowering of the potential barrier by an effective work function, that matched the results of Feng and Verboncoeur quite well. Other recent work includes a three dimensional theory for space-charge effects on field emission from a Spindt type emitter¹¹ and on space-charge and quantum effects¹².

The work presented in this paper was motivated by the desire to use molecular dynamics methods to simulate electron beams in vacuum micro- and nanoelectronics devices. An advantage of this approach is that it can account more accurately for collisional effects than simulations based on fluid models or particle-in-cell codes. A disadvantage is the high computational cost, but in the small systems that are of interest, the number of free

electrons is small enough that this is not an issue. Previous work in this area¹³⁻¹⁵ has been based on something akin to photoemission as the source of electrons, whereby the surface electric field does not directly affect the rate of electron emission from the cathode although space-charge effects do limit the current via virtual cathode formation. Due to the importance of field emission it is desirable to implement that type of emission process in the molecular dynamics code being used for simulation of vacuum nanoelectronics devices.

In this paper we present a field emission model based on image-charge considerations that is suitable for the molecular dynamics approach. We show how this model can replicate already established results, particularly with regard to space-charge effects, and we use our model to simulate field emission in a planar diode of limited emitter area. The simulation results are then compared to a simple fluid model for field emission from a planar emitter of finite area.

Section II of this paper gives a description of the model and simulation methodology used. Simulation results are presented in Section III followed by a fluid model description of two-dimensional effects in field emission in Section IV and finally by a short summary and discussion in Section V.

II. METHODOLOGY

The model used is a planar vacuum diode with gap width d as is depicted in Fig. 1. The potential at the cathode is zero and the anode potential is V_0 . Field emission is only allowed to take place from a finite square-shaped area on the cathode surface. Both the cathode and anode surfaces are infinite. The side length, L , of this square emitter region is smaller than the gap spacing d . A molecular dynamics (MD) approach is used to calculate electron motion and is the basis for the field emission algorithm. The simulation is of high resolution in the sense that every single electron present in the vacuum gap is treated as an individual particle. The Coulomb field due to every electron in the system along with the image-charge partners on either side of the cathode/anode are taken into account. Thus the total field at any point is

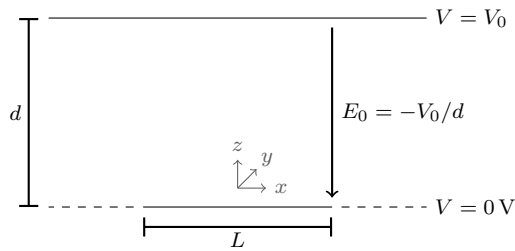


FIG. 1. The model of the planar nanodiode.

$E = E_{sc} + E_0$, where E_{sc} is the detailed space-charge field and E_0 is the vacuum field. Particle advancement is calculated using Verlet integration with a time step of 0.1 fs.

Field emission is a quantum mechanical tunnelling process which can be described with the Fowler-Nordheim equation³

$$J = \frac{A}{t^2(\ell)\phi} F^2 e^{-\nu(\ell)B\phi^{\frac{3}{2}}/F}, \quad (1)$$

where ϕ is the work-function and F is the field at the surface of the cathode, taken to be positive. $A = e^2/(16\pi^2\hbar)$ [A eV V^{-2}] and $B = 4/(3\hbar)\sqrt{2m_e e}$ [$\text{eV}^{-\frac{3}{2}} \text{V m}^{-1}$] are the first and second Fowler-Nordheim constants, while $\nu(\ell)$ is called the Nordheim function and arises due to the image-charge effect. It contains complete elliptic integrals of the first and second kind and is related to $t(\ell)$ by the relation $t(\ell) = \nu(\ell) - (4/3)\ell d\nu(\ell)/d\ell$. Approximations found by Forbes and Deane⁴,

$$\nu(\ell) = 1 - \ell + \frac{1}{6}\ell \ln(\ell) \quad (2a)$$

and

$$t(\ell) = 1 + \ell \left(\frac{1}{9} - \frac{1}{18} \ln(\ell) \right) \quad (2b)$$

are used, where

$$\ell = \frac{e}{4\pi\epsilon_0} \frac{F}{\phi^2}. \quad (2c)$$

Image-charge is taken into consideration with two objectives in mind. First, to maintain the proper boundary conditions at the cathode we include image-charge partners for the space-charge to be found in the gap. Second, the image-charge of the electron being emitted is taken into account in calculating the barrier potential which the electron must tunnel through. This can be seen in Fig. 2 where the bare triangular (BT) barrier is given by $U^{BT}(z) = \phi - eFz$ and the screened Schottky-Nordheim (SN) barrier by $U^{SN}(z) = \phi - eFz - e^2/(16\pi\epsilon_0 z)$. The SN barrier contains an additional term which arises due to the image-charge effect. Tunnelling is more pronounced due to this term because the barrier

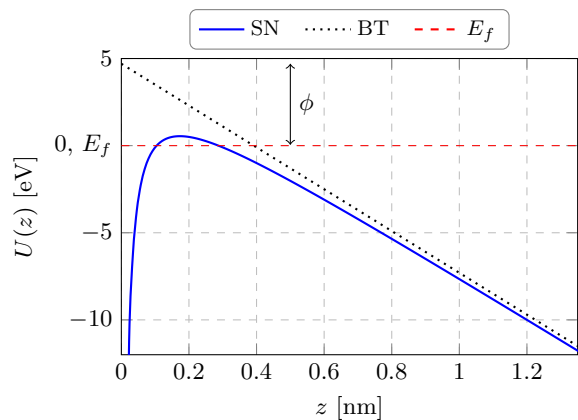


FIG. 2. The bare triangular barrier vs. the Schottky-Nordheim barrier for field emission.

height and width are reduced compared to the triangular barrier.

Numerical methods are used to obtain the dynamics in the system. The total number of electrons in the system is not constant since electrons are continuously entering the system at the cathode and leaving at the anode. The Metropolis-Hastings algorithm¹⁶ is used to sample the surface electric field to find a favourable locations for emission. The probability of emission $D_F = \exp(-\nu(\ell)B\phi^{\frac{3}{2}}/F)$, is then evaluated for small areas at those locations in order to determine whether emission occurs. The current density emitted from the cathode is normalized such that Fowler-Nordheim current density is obtained. Relativistic effects and radiation caused by acceleration of electrons are safely neglected as all occurring velocities are much smaller than the speed of light.

III. RESULTS OF THE MD SIMULATIONS

A. Current-voltage characteristic

We start by examining a system with a work function of $\phi = 4.7 \text{ eV}$. The value is chosen because many metals have a work function in the range from 4.5 eV to 5.0 eV. This work function might represent Copper (Cu), Tungsten (W) or other metals. The gap spacing $d = 2500 \text{ nm}$ and voltage $V = 20\text{--}35 \text{ kV}$ were then selected such that the vacuum field was sufficient to obtain field emission. Care was taken in selecting the vacuum field such that the parameter ℓ in Eq. 2c was less than 1. If ℓ is larger than 1 then the barrier in Fig. 2 will be below the Fermi energy. A higher work function means that a higher surface field is required to obtain field emission. In Fig. 3 the current density is plotted as a function of the voltage on a log scale. It shows the exponential increase as is expected from the Fowler-Nordheim equation. The red dashed line shows the Fowler-Nordheim theory (Eq. 1) without space-charge effects. The blue solid line represents the results from the simulations in the steady

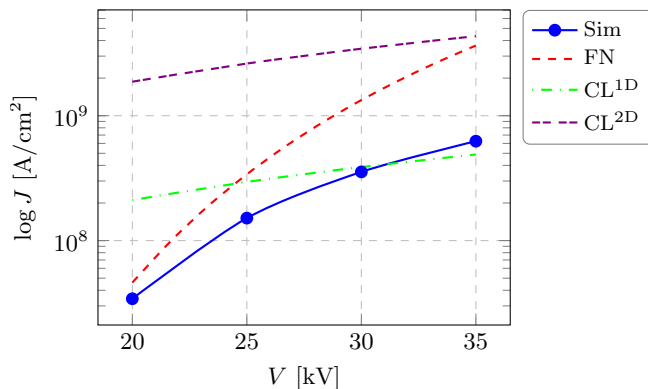


FIG. 3. The current density plotted on a log scale vs. the voltage in the system. The **red** dashed curve shows the results using the value of the vacuum field in the Fowler-Nordheim equation, and the **blue** solid curve shows the results from the simulations. While the **green** dot dashed and **violet** double dashed curves represent the 1D and 2D¹⁹ CL limits respectively. The parameters used in the simulation were $\Phi = 4.7$ eV, $d = 2500$ nm and $L = 100$ nm.

state. We see that it is lower than the values given by the Fowler-Nordheim theory. This is due to space-charge effects lowering the surface field at the cathode and reducing the emission. The **green** dot dashed curve shows the 1D Child-Langmuir (CL)^{17,18} limit and the double dashed **violet** is the 2D CL limit derived by Lau¹⁹. We see that under high voltage it is possible to go over the 1D CL limit but the 2D limit is still far off.

B. Surface field at the cathode

In order to verify the code we use for our simulations, we compared our results to Particle in Cell (PIC) simulations. In reference 2 Feng and Verboncoeur do 1D PIC simulations to study space-charge limited current with Fowler-Nordheim field emission. Using the same parameters as they do, $\phi = 2.0$ eV, $V = 2$ kV and $d = 1000$ nm, we obtain Fig. 4, which shows the average surface field on the cathode similar to Fig. 4 in the paper by Feng and Verboncoeur. The **blue** lines represent the average surface field for different side lengths L of the active region on the cathode. The values used are $L = 50, 100, 200, \dots, 1000, 2500$ nm. The magnitude of the steady state field decreases as the side length increases, because the space-charge effects increase. For a large side length, comparable to the gap space, the field resulting from our MD simulations approaches the 1D limit obtained in the steady state by the PIC method, which we plotted as the black line.

The surface field shows time dependent oscillations, both in the MD and PIC simulations, before it settles down into the steady state. The oscillations resulting from the PIC method are not shown here (see Figure 4 of Ref.²), but they are very similar to ours for $L = 2500$ nm

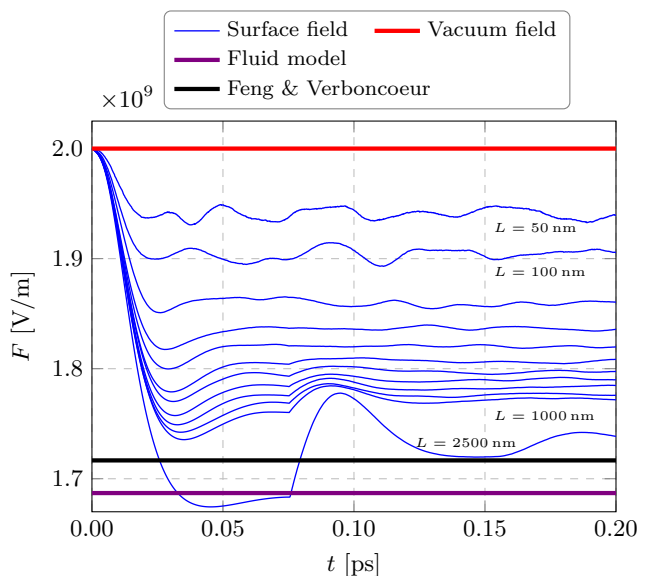


FIG. 4. Average surface field plotted for different side lengths, $L = 50, 100, 200, \dots, 1000, 2500$ nm. The magnitude of the steady-state field decreases with increasing L . Other parameters were $\phi = 2.0$ eV, $V = 2$ kV and $d = 1000$ nm.

and $t > 0.1$ ps. However, an interesting feature is present in the MD simulations, but not visible in the PIC results: it is the sudden increase in the surface field seen at around $t \approx 0.075$ ps, like a kink growing with increasing cathode size. This time corresponds to the transit time of the electrons in the system and is the moment when the first electrons are being absorbed at the anode. The large number of electrons that were emitted in beginning are now being absorbed which then cause the surface field to increase abruptly as the absorbed electrons leave the system. The effect is more pronounced for larger side lengths because of the higher number of electrons in the system being emitted and absorbed.

The Coulomb oscillations become faster and denser for a small cathode size because of the larger fluctuations of the emitted charge in combination with the self consistent space-charge. Such oscillations may eventually split the electron beam into bunches if the emission process can be sufficiently fast as in the photoemission case¹³. In our present approach the diode is initially empty and a large number of electrons can be emitted in the first time steps. In this regime, i. e. for $t < 0.01 - 0.02$ ps, the space-charge effects are small. After the field reaches its lowest magnitude it starts to increase slightly again because the electron are moving away from the cathode and towards the anode. The oscillations in the field slowly die away with time. In our Fig. 4 the vacuum field is represented by the red line and the violet line shows the equilibrium surface field obtained by the fluid model described in Section IV.

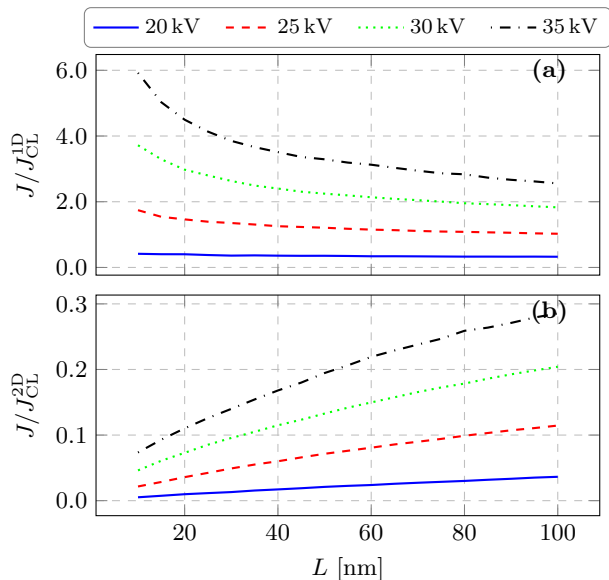


FIG. 5. (a) The current density scaled with the 1D Child-Langmuir limit. (b) The current density scaled with the 2D Child-Langmuir from Lau¹⁹ as a function of the side length L for different voltages. Other parameters used were $\Phi = 4.7$ eV and $d = 2500$ nm.

C. Current vs. cathode size

In Fig. 5(a) we see the current density scaled with the 1D Child-Langmuir limit and in Fig. 5(b) scaled with the 2D Child-Langmuir limit from Lau¹⁹ as a function of the side length $L = 10$ –100 nm. The current density decreases as the size of the active emission area on the cathode increases, and approaches an asymptotic value for an infinite area. This can be easily understood since, as is the case with Child-Langmuir emission from a 2D emitter, the surface field has its lowest magnitude in the center of the emitter and increases towards the edges²⁰. The contribution of the edge electrons to the surface field will be less and less as the emitter area increases due to the inverse square nature of Coulomb’s law. The current density will therefore, asymptotically approach some final value as the active emission area increases.

D. Beam distribution

Fig. 6 shows the distribution of the transit time of the electrons through the gap. The distribution is approximately a Gaussian with a FWHM ≈ 0.07 fs, and a peak at $t = 53.5$ fs. From energy conservation the estimated transit time for a single electron over the gap is $\Delta t = \sqrt{2m_e d^2 / (V_0 e)} \approx 53.32$ fs, which is not far from the peak value of the distribution. It is the Coulomb interaction in the system that slightly shifts the peak from the single electron value and gives the width of the distribution. The width of the peak is small, which indicates that the electrons travel quite fast over the gap and do

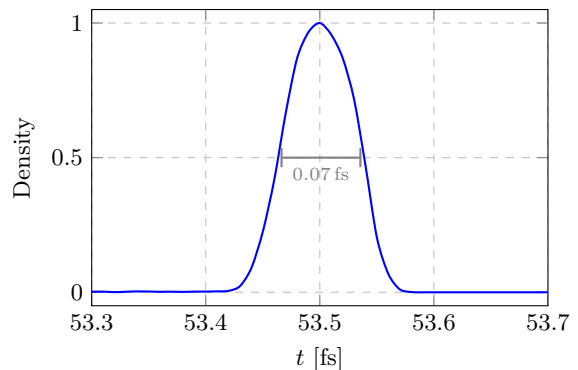


FIG. 6. Distribution of the transit time of the electrons through the gap for $V = 25$ kV, $d = 2500$ nm and $\phi = 4.7$ eV.

not have a lot of time to interact and spread out.

Fig. 7 shows the absorption profile on the anode surface. The inner white square represents the active emission area on the cathode, while the outer white square shows the boundaries of the absorbed electrons on the anode. The Coulomb interaction slightly rounds the corners of the beam from the square shape of the emitter. The side length of the outer square is about 2×32.25 nm larger than the inner square which has $L = 100$ nm. This means that beam spreading is small compared with the gap spacing, $d = 2500$ nm.

IV. FLUID MODEL

A simpler method that can be used to describe the field emission is by calculating the electric field in the diode from the charge density. The charge density can be estimated by combining the continuity equation, $\rho(z)p/m_e = J$, where p is the momentum, and the conservation of energy $p^2/(2m_e) = eV_0 z/d$, which gives

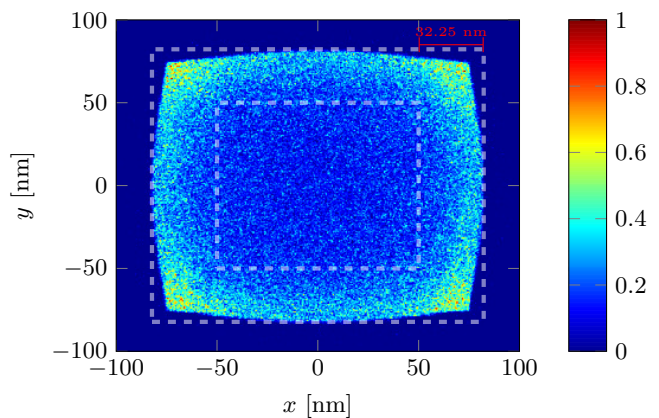


FIG. 7. Absorption profile at the anode. Inner box shows the emitter size while the outer box shows the edge of the beam on the absorption plane. Parameters used were $\Phi = 4.7$ eV, $d = 2500$ nm and $V = 30$ kV.

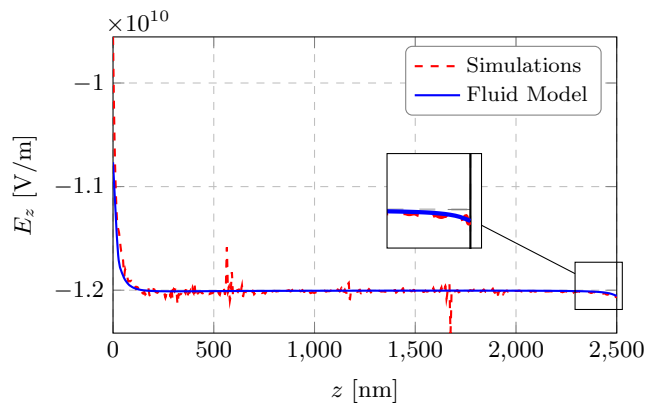


FIG. 8. The electric field in the z -direction through the center of the diode. $V = 30$ kV, $d = 2500$ nm and $\phi = 4.7$ eV. Inset shows the electric field near the anode.

$\rho(z) = J\sqrt{m_e d / (2eV_0 z)}$. Note that we have made use of the vacuum potential to calculate the charge density. This proves to be a sufficient approximation for the situation that is being studied where the current density is still considerably lower than the 2D Child-Langmuir current density (as can be seen from Fig. 5). When the current density approaches the Child-Langmuir current density an iterative calculation of the potential as a function of z can be used instead, at added computational cost. This charge density is distributed over the whole diode and therefore it behaves more like a fluid than like a collection of single particles. It also assumes the beam does not spread too much laterally, which is a fair approximation in our system as can be seen in Fig. 7.

Once the charge density is known it is easy to write down the equation for the z -component of the electric field through the center of the diode,

$$\hat{E}_{\text{sc}}^{\pm}(\hat{z}) = \frac{\hat{J}}{9\pi} \int_0^1 \int_{-\frac{\hat{z}}{2}}^{\frac{\hat{z}}{2}} \int_{-\frac{\hat{z}}{2}}^{\frac{\hat{z}}{2}} \frac{\hat{z}' \pm \hat{z}}{\sqrt{\hat{z}'^2 + \hat{y}'^2 + (\hat{z}' \pm \hat{z})^2}^{\frac{3}{2}}} d\hat{x}' d\hat{y}' d\hat{z}', \quad (3)$$

where $\hat{E} = E/(-V_0/d)$, $\hat{J} = J/J_{\text{CL}}^{\text{2D}}$ and \hat{x} , \hat{y} and \hat{z} are scaled using the gap spacing d . The plus sign in the integral is used when calculating the image-charge effect and the minus sign for the field in the diode. The total field is then $\hat{E}_z(\hat{z}) = 1 - \hat{E}_{\text{sc}}^+(\hat{z}) - \hat{E}_{\text{sc}}^-(\hat{z})$.

In Fig. 8 we see the z -component of the electric field through the center of the diode plotted as a function of the z -coordinate (distance from the cathode). The red dashed curve shows a typical result of an MD simulation snapshot at a fixed time step, while the blue solid curve shows our fluid like model calculated using Eq. 3 with numerical integration. The value of the current density used, J , is taken from the simulation. The fluctuations in the field from the simulations are due to electrons that are close to the center line where the field is being calculated. The fluid model fits quite well with the simulation results.

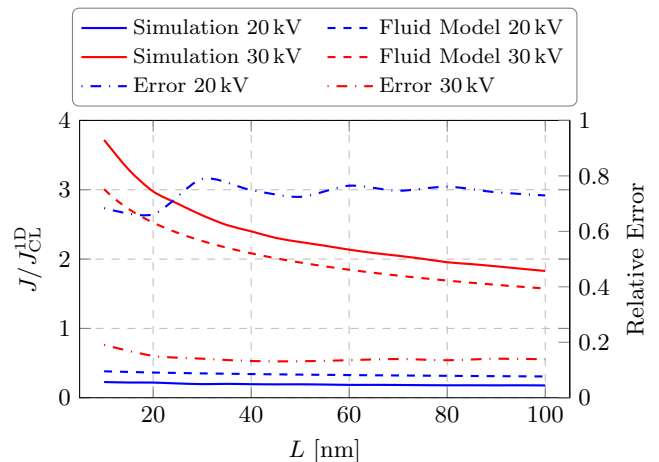


FIG. 9. Comparison of the current density between the MD simulation (solid curves) and the fluid model (dashed curves) for $V = 20$ kV (bottom blue curves) and $V = 30$ kV (top red curves). Other parameters used were $d = 2500$ nm and $\phi = 4.7$ eV.

The derivative of the electric field is proportional to the charge density, $\rho(z)$, which is highest near the cathode, where most of the electrons are located. The electrons are injected with zero-velocity and consequently spend more time near the cathode before being accelerated over the gap. The electrons spread out as their velocity increases, and therefore the charge density decreases rapidly and the electric field levels off after the electrons have travelled roughly the distance of the side length L away from the cathode. The electric field decreases slightly at the end of the gap, near the anode, due to the absorption of the electrons into the anode. There is no charge accumulated at the anode, which causes the field to drop slightly. Image-charge partners are included in the simulations at the anode, but not in the fluid model. It appears that the image-charge contributes little to the field near the anode.

It is also possible to use the fluid model to calculate the current density from the cathode. This is done by iterations, using Eq. 1 and 3. The vacuum field is used as an initial value for the field in Eq. 1. The value obtained is then scaled using the Child-Langmuir limit and put into Eq. 3 with $z = 0$, which gives a new value for the surface field in center of the cathode. This procedure is repeated until the current density has converged.

In Fig. 9 we see a comparison between the fluid model and the simulation results for calculating the current density emitted. The blue solid curve shows the simulation results, while the red dashed the fluid model calculate using method just described. It is expected that the fluid model would give slightly lower results. The model calculates the surface field in the center of the diode and as was explained earlier the field is lower there than at the edges. The fluid model therefore underestimates the current density emitted from the edges.

In Fig. 10 we see the results of the fluid model

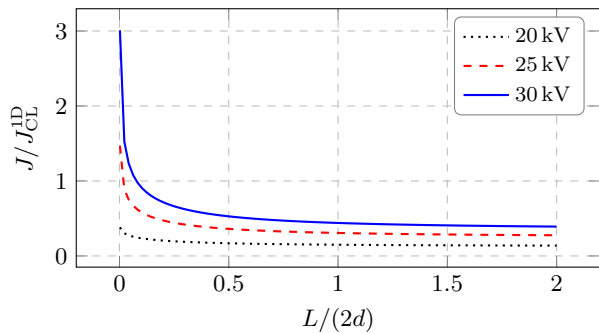


FIG. 10. Results of the fluid model for different values of the voltage as a function of the side length. $L = 10\text{--}10.000\text{ nm}$ with $d = 2500\text{ nm}$ and $\phi = 4.7\text{ eV}$.

for different values of the voltage as a function of $L = 10\text{--}10.000\text{ nm}$ with $d = 2500\text{ nm}$ and $\phi = 4.7\text{ eV}$. The results are qualitatively the same as in Fig. 5(b). The fluid model allows us to estimate the current density for diodes with a larger emitting area and see the asymptotic behaviour better with calculations that can be done in a few hours, whereas the MD simulations would require weeks of computational time for the same parameters. The shape of the curves seen is very similar to the current profile seen in space-charge limited flow from circular cathodes²¹.

V. SUMMARY AND CONCLUSIONS

We performed molecular dynamics (MD) simulations of electrons in a diode where the electrons are extracted from the cathode by the field emission mechanism. The emission is essentially governed by the quantum mechanical tunnelling through the potential barrier associated with the surface of the metallic cathode, which leads to the well known Fowler-Nordheim law for an infinite planar diode.

Our results include space-charge effects and are in good agreement with the results obtained by other authors^{2,10}. In particular they are in good agreement with the PIC simulations. MD simulations are more computationally expensive than PIC simulations, but are more accurate. In the MD simulation every particle is tracked precisely and the force on it is calculated exactly, using the Coulomb interaction from all other particles in the system. Whereas in PIC simulation the system is divided up into a grid and the field in each section of the grid is the mean field of the particles in that section. The only methodological approximation in the MD simulations is the finite time step, which must be chosen much smaller than the characteristic time of the beam dynamics.

Time dependent oscillations of the electric field are obtained during the transient period after the diode is switched on. A kink of cathode field is obtained as a response to the charge fluctuation produced when the first electrons are absorbed at the anode.

The MD method is best suited when the number of the electrons in the diode is not too large, typically below few thousands. For larger numbers it becomes computationally prohibited, but in those cases the mean field results like those of PIC calculations, are usually accurate.

We derive a relatively simple fluid model of the electron beam, which incorporates the essential electrostatics, where the electric field is derived self consistently with an estimated continuous charge distribution, and with the image-charge induced at the cathode and at the anode. The results of the fluid model are in good agreement with those of the MD simulations. We can use this fluid model to estimate the effects of finite emitter area over a wide range of parameters. We observe that the current density for field emission from a finite emitter with space-charge effects included, is qualitatively similar to Child-Langmuir emission from a finite emitter area, in that the current density increases with diminishing emitter area.

ACKNOWLEDGMENTS

This work was financially supported by the Icelandic Research Fund grant number 120009021. The simulations were performed on resources provided by the Nordic High Performance Computing (NHPC).

- ¹Y. Y. Lau, Y. Liu, and R. K. Parker, *Physics of Plasmas* (1994-present) **1**, 2082 (1994).
- ²Y. Feng and J. P. Verboncoeur, *Physics of Plasmas* (1994-present) **13**, 073105 (2006).
- ³R. H. Fowler and L. Nordheim, *Proceedings of the Royal Society of London. Series A* **119**, 173 (1928).
- ⁴R. G. Forbes and J. H. Deane, *Proceedings of the Royal Society A: Mathematical, Physical and Engineering Science* **463**, 2907 (2007).
- ⁵K. L. Jensen, *Journal of Vacuum Science & Technology B* **21**, 1528 (2003).
- ⁶J. A. Eichmeier and M. Thumm, eds., *Vacuum electronics: Components and Devices* (Springer, 2008).
- ⁷W. Zhu, ed., *Vacuum Microelectronics* (John Wiley & Sons, 2004).
- ⁸A. Neuber, L. Laurent, Y. Lau, and H. Krompholz, *Windows and RF Breakdown*, edited by R. Barker and E. Schlamigolu (Wiley-IEEE Press, 2001) pp. 325–375, chapter 10 in High-Power Microwave Sources and Technologies.
- ⁹J. P. Barbour, W. W. Dolan, J. K. Trolan, E. E. Martin, and W. P. Dyke, *Phys. Rev.* **92**, 45 (1953).
- ¹⁰A. Rokhlenko, K. L. Jensen, and J. L. Lebowitz, *Journal of Applied Physics* **107**, 014904 (2010).
- ¹¹K. L. Jensen, *Journal of Applied Physics* **107**, 014905 (2010).
- ¹²K. L. Jensen, J. Lebowitz, Y. Y. Lau, and J. Luginsland, *Journal of Applied Physics* **111**, 054917 (2012).
- ¹³A. Pedersen, A. Manolescu, and A. Valfells, *Phys. Rev. Lett.* **104**, 175002 (2010).
- ¹⁴P. Jonsson, M. Ilkov, A. Manolescu, A. Pedersen, and A. Valfells, *Physics of Plasmas* (1994-present) **20**, 023107 (2013).
- ¹⁵M. Ilkov, K. Torfason, A. Manolescu, and A. Valfells, *Electron Devices, IEEE Transactions on* **62**, 200 (2015).
- ¹⁶W. K. Hastings, *Biometrika* **57**, pp. 97 (1970).
- ¹⁷C. D. Child, *Phys. Rev. (Series I)* **32**, 492 (1911).
- ¹⁸I. Langmuir, *Phys. Rev.* **2**, 450 (1913).
- ¹⁹Y. Y. Lau, *Phys. Rev. Lett.* **87**, 278301 (2001).

²⁰J. W. Luginsland, Y. Y. Lau, R. J. Umstattd, and J. J. Watrous, *Physics of Plasmas (1994-present)* **9**, 2371 (2002).

²¹B. Ragan-Kelley, J. Verboncoeur, and Y. Feng, *Physics of Plasmas (1994-present)* **16**, 103102 (2009).